

Supplementary material for:

**Enhanced spin-orbit torque and field-free switching in Au/TMDs/Ni hybrid structures**

Yi Luo<sup>1,2</sup>, Qian Chen<sup>2\*</sup>, Rongxin Li<sup>2</sup>, Yipeng Wang<sup>2</sup>, Weiming Lv<sup>2</sup>, Baoshun Zhang<sup>2</sup>, Yaming Fan<sup>3</sup>, Hao Wu<sup>4\*</sup> and Zhongming Zeng<sup>1,2,3\*</sup>

<sup>1</sup> School of Nano-Tech and Nano-Bionics, University of Science and Technology of China, Hefei, Anhui 230026, People's Republic of China

<sup>2</sup> Nanofabrication facility, Suzhou Institute of Nano-Tech and Nano-Bionics, Chinese Academy of Sciences, Suzhou, Jiangsu 215123, China

<sup>3</sup> Division of Nano-Devices and Technologies & Nanchang Key Laboratory of Advanced Packaging, Jiangxi Institute of Nanotechnology, SINANONC, Nanchang 330200, China

<sup>4</sup> Songshan Lake Materials Laboratory, Dongguan, Guangdong 523808, China.

**\*Corresponding Authors:**

zmzeng2012@sinano.ac.cn, qchen2016@sinano.ac.cn, wuhao1@sslslab.org.cn

**Contents:**

S1. The surface topography of Au

S2. Parallel resistor model and Oersted field in devices

S3. ST-FMR measurements of Au/Ni

S4. DC bias resonance linewidth and the resonance field

S5. ST-FMR measurements with different in-plane magnetic-field angles;

S6. Spin Hall conductivity of Au/MX<sub>2</sub>/Ni

## S1. The surface topography of Au

The surface topography and thickness of TMDs are measured by atomic force microscopy (AFM) which are shown in text. Figure S1 shows the surface topography of Au and the arithmetic mean deviation of roughness profile is  $R_a=0.594\text{nm}$  which indicates the great quality and the continuity of Au.

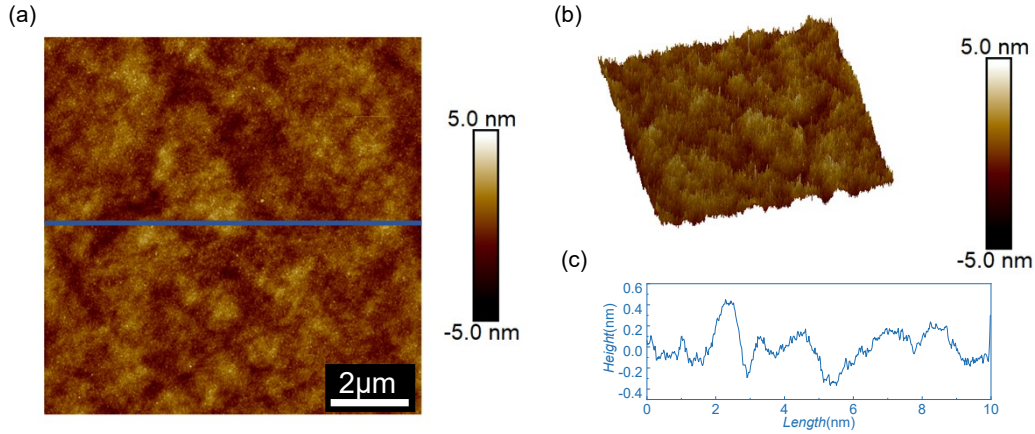


**Figure S1. The surface topography of Au by AFM with tapping mode.** (a) 2D image. (b) 3D image. (c) Corresponding to the change in height at the straight line in (a).

## S2. Parallel resistor model and Oersted field in devices

As the thickness of the film is decreased to a few atomic layers, the conductivity drops below that of the bulk metal.<sup>[1]</sup> Therefore, it is necessary to know the conductivity of Au (4 nm) and Ni (6 nm) films respectively.

As shown in the inset of Figure S1(a) and (b), Ti(2 nm)/Au(4 nm) and Ti(2 nm)/Au(4 nm)/Ni(6 nm) films are fabricated into Hall devices. The conductivities are measured by four-probe method, and Figure.S1 (a) and (b) show  $I$ - $V$  curves of devices. To ensure accuracy, 5 devices are measured for each kind of structure (Figure S1(c) shows). It is noted that current shunts on 2 nm Ti and monolayered TMDs are ignored, due to the much larger resistivity of Ti and TMDs compared with Au. We obtain average values of resistance ( $R$ ) are  $R_{Au/Ni} = 93\Omega$  and  $R_{Au} = 180\Omega$ .

$$\sigma = \frac{L}{RS} \quad (S1)$$

$$\frac{1}{R_{Au/Ni}} = \frac{1}{R_{Au}} + \frac{1}{R_{Ni}} \quad (S2)$$

where  $R_{Au/Ni}$ ,  $R_{Au}$ , and  $R_{Ni}$  are the resistance of Au/Ni, Au and Ni respectively,  $\sigma$  is the conductivity,  $L$  is the length of current flow and  $S$  is the cross-section perpendicular to the direction of current. Considering devices as a parallel resistors system according to (Eq. S1) and (Eq. S2), the calculated conductivity is  $\sigma_{Au(4)} = 5.152 \times 10^6 (\Omega \cdot \text{m})^{-1}$ ,  $\sigma_{Ni(6)} = 1.344 \times 10^6 (\Omega \cdot \text{m})^{-1}$ .

From the conductivities of each layer, we can evaluate the current distribution in the device. According to Eq. S3, we calculated that about 72% of the current flows through the Au layer, and the current density in Au layer is about  $2.3 \times 10^{10} \text{ A} \cdot \text{m}^{-2}$  by Eq. S4.

$$\frac{I_{Au}}{I_{Ni}} = \frac{d_{Au}\sigma_{Au}}{d_{Ni}\sigma_{Ni}} \quad (S3)$$

$$J_{Au} = \frac{I_{Au}}{S_{Au}} \quad (S4)$$

where  $I_{Au}$  and  $I_{Ni}$  are the currents passing through the Au and Ni, respectively,  $J_{Au}$  is the current density of Au. Based on the estimated charge-current densities in the each layer, we obtain Oersted field  $H_{Oe} = \frac{1}{2}(J_{Au}t_{Au}) = 0.59$  Oe/mA, where  $t_{Au}$  is the thickness of Au.<sup>[2]</sup>

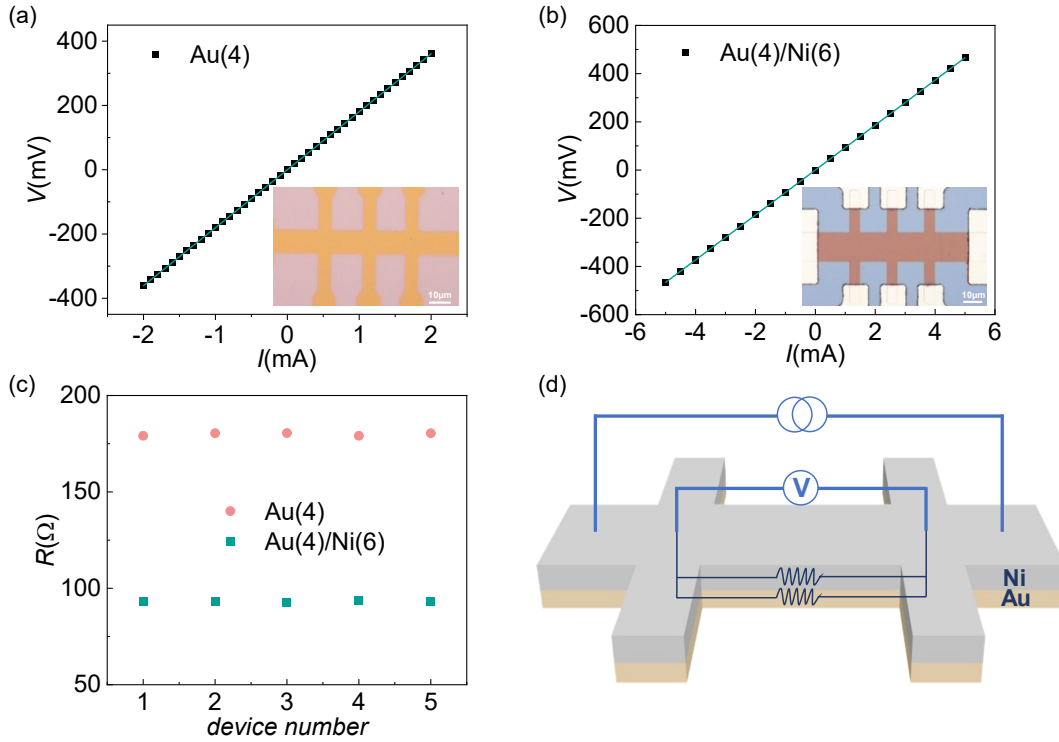


**Figure S2. Conductivity measurements of Ti(2 nm)/Au(4 nm) and Ti(2 nm)/Au(4 nm)/Ni(6 nm).** I-V curves of (a) Ti(2 nm)/Au(4 nm). (b) Ti(2 nm)/Au(4 nm)/Ni(6 nm). Insets show optical microscopy images of corresponding devices. (c) Resistances of Ti(2 nm)/Au(4 nm) and Ti(2 nm)/Au(4 nm)/Ni(6 nm). (d) Abridged general view of four-probe method measurements setup with samples.

### S3. ST-FMR measurements of Au/Ni

In order to study the role of the two-dimensional transition metal dichalcogenides (2D TMDs) inserts, DC-tuned ST-FMR curve of Au/Ni is measured. By fitting the ST-FMR curve (Eq. 1 mentioned in main text), we obtain the linear change of the linewidth  $\delta\Delta H$  and the resonance field  $\delta H_r$  versus  $I_{dc}$  (Figure S2 shows) for positive ( $45^\circ$ ) and negative ( $-135^\circ$ ) magnetic fields respectively.

The slopes of curves for the two field directions are almost equal ( $-0.32$  and  $0.30$  Oe/mA for  $\delta\Delta H$ ,  $-1.87$  and  $1.67$  Oe/mA for  $\delta H_r/\sin\phi$ ), which substantiates that samples are magnetized in the opposite direction and the polarity of the damping-like torque is reversed by the reversion of the external field (from  $\phi = 45^\circ$  to  $-135^\circ$ ,  $\phi$  is the angle between external field and  $I_{dc}$ ) and the predominance of conventional SOTs. At the same time, we calculate

$\xi_{DL,eff}$  and  $\xi_{FL,eff}$  of Au/Ni through Eq. 2 and Eq. 3 respectively, which are listed in Table S1.

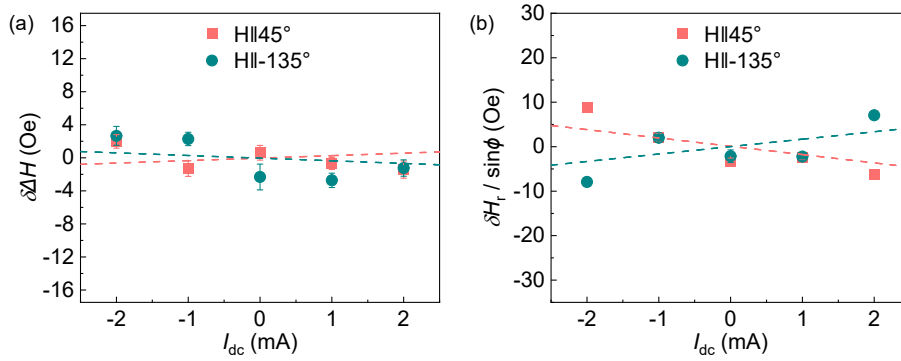


**Figure S3. ST-FMR measurement of Au(4)/Ni(6) with different dc-bias at room temperature.** Corresponding variations at 3 GHz of (a) the resonance linewidth and (b) the resonance field.

**Table S1. Efficiencies of damping-like and field-like SOTs calculated by dc-tuned method**

Structure	$\xi_{DL,eff}(45^\circ)$	$\xi_{DL,eff}(-135^\circ)$	$\xi_{FL,eff}(45^\circ)$	$\xi_{FL,eff}(-135^\circ)$
Au/Ni	0.0281±0.0169	0.0299±0.0197	0.0546±0.0398	0.0465±0.0423
Au/ML WTe <sub>2</sub> /Ni	0.2136±0.0159	0.3701±0.0240	0.1862±0.0177	0.2192±0.0331
Au/ML MoS <sub>2</sub> /Ni	0.2916±0.0310	0.5095±0.0374	0.3963±0.0359	0.3060±0.0275

#### S4. DC bias resonance linewidth and the resonance field

Both the linewidth and the resonance field of Ni versus the applied DC current  $I_{dc}$  are showed in Figure 2 and Figure S2. There are significant variations of the linewidth  $\delta\Delta H$  and the resonance field  $\delta H_r$  for Au/MX<sub>2</sub>/Ni devices, and the variation values are listed in Table S2. Compared to Au/Ni,  $\delta\Delta H$  at 45° and -135° have increased 7.57 and 12.28 times for Au/WTe<sub>2</sub>/Ni. For Au/MoS<sub>2</sub>/Ni,  $\delta\Delta H$  at 45° and -135° have increased 10.93 and 17.90 times. At 45° and -135°, the slope of  $\delta H_r$  increases to 3.41 and 4.71 times for Au/WTe<sub>2</sub>/Ni and 7.26 and 6.58 times for Au/MoS<sub>2</sub>/Ni respectively. Not only do these variation values indicate the large damping-like and field-like SOTs but also the asymmetry of devices result from TMDs inserts.

**Table S2. Extracted values of  $\delta\Delta H$  and  $\delta H_r$**

Structure	$\delta\Delta H(45^\circ)$ (Oe/mA)	$\delta\Delta H(-135^\circ)$ (Oe/mA)	$\delta H_r/\sin\phi(45^\circ)$ (Oe/mA)	$\delta H_r/\sin\phi(-135^\circ)$ (Oe/mA)
Au/Ni	0.30 ± 0.35	-0.32 ± 0.35	-1.87 ± 0.99	1.67 ± 1.05
Au/ ML WTe <sub>2</sub> / Ni	2.27 ± 0.16	-3.93 ± 0.23	-5.12 ± 0.44	5.94 ± 0.82
Au/ ML MoS <sub>2</sub> / Ni	3.28 ± 0.35	-5.73 ± 0.41	-10.32 ± 0.89	8.09 ± 0.68

## S5. ST-FMR measurements with different in-plane magnetic-field angles

To further demonstrate the unconventional out-of-plane damping-like SOT in Au/TMDs/Ni structures, we analyze the angular dependence of  $V_S$  and  $V_A$ . Because of the high-symmetry of Au, conventional SOTs consist of an out-of-plane field-like torque,  $\vec{\tau}_A \propto \hat{m} \times \hat{y}$ , and an in-plane damping-like torque,  $\vec{\tau}_S \propto \hat{m} \times (\hat{m} \times \hat{y})$ , so that  $V_A$  and  $V_S$  conform to the angle dependence of  $\sin(2\phi) \cos(\phi)$ . Here we define the applied current as always being in the  $\hat{x}$  direction, and the film normal is in the  $\hat{z}$  direction. The unconventional out-of-plane damping-like torque  $\vec{\tau}_B$  can be fitted from the angular dependence of  $V_a$  by adding a term  $\Delta V_a$  proportional to  $\sin(2\phi)$ <sup>[3]</sup>:

$$V_a(\phi) = A \cos(\phi) \sin(2\phi) + B \sin(2\phi) \quad (\text{S5})$$

As shown in Figure S3, there is  $\Delta V_a$  in Au/TMDs/Ni but not in Au/Ni, which is the evidence of the unconventional out-of-plane damping-like SOT Au/TMDs/Ni. This proves that TMDs inserts contribute to the formation of out-of-plane component of the spin polarization, because of the strong hybridization at TMDs/Ni interface.

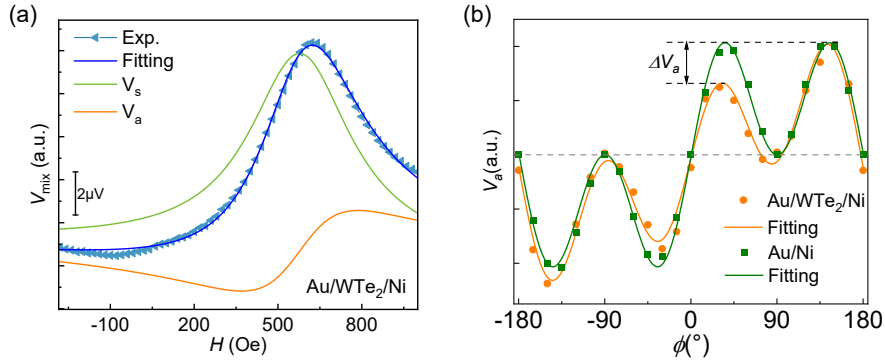


**Figure S4 (a)** Measured ST-FMR spectra for Au/WTe<sub>2</sub>/Ni, with the magnetization oriented at 30° relative to the current direction and  $f = 3$  GHz. The lines are fits to Eq. 1 showing the symmetric  $V_s$  and antisymmetric  $V_a$  components. **(b)**  $V_a$  as a function of in-plane magnetic-field angle ( $\phi$ ) for Au/WTe<sub>2</sub>/Ni and Au/Ni.

## S6. Spin Hall conductivity of Au/MX<sub>2</sub>/Ni

For some TMDs, although the spin-charge conversion efficiency is high enough, the conductivity is too low to avoid power consumption. Therefore, we calculated the spin Hall conductivity ( $\sigma^{SH}$ ) of Au, Au/WTe<sub>2</sub> and Au/MoS<sub>2</sub> by  $\sigma^{SH} = \sigma_{xx} \theta_{DL}$ , where  $\sigma_{xx}$  is the conductivity and  $\theta_{DL}$  is the effective spin-Hall angle representing the effects of the conventional and unconventional damping-like torques. When  $\phi = -135^\circ$ ,  $\sigma^{SH}$  shows the combined effects of the conventional and unconventional components. When  $\phi = 45^\circ$ ,  $\sigma^{SH}$  denotes the equalizing influence of the two components. As for the conductivity, we mainly take the conductivity of Au ( $\sigma_{xx} = 0.5152 \times 10^7$  ( $\Omega \text{ m}$ )<sup>-1</sup>) as the conductivity of Au/WTe<sub>2</sub> and Au/MoS<sub>2</sub>, because there are about 98.76% and 99.90% current flows through Au in Au/WTe<sub>2</sub> and Au/MoS<sub>2</sub> respectively. Table S3 shows the  $\sigma^{SH}$  of Au, Au/WTe<sub>2</sub> and Au/MoS<sub>2</sub>. It is clearly that  $\sigma^{SH}$  is increased by an order of magnitude after inserting TMDs. Figure S4 shows  $\sigma^{SH}$  of previous work and our work,

from which we can see that the spin Hall conductivity of Au/TMDs is higher than other materials. Crucially, the  $\sigma_{SH}$  of Au/MoS<sub>2</sub> is more than 60 times larger than Pt ( $0.04 \times 10^6 \sim 0.5 \times 10^6 [(\hbar/2e) (\Omega \text{ m})^{-1}]$ )<sup>[4-6]</sup> and an order of magnitude higher than PtTe<sub>2</sub> ( $0.2 \sim 1.6 \times 10^5 [(\hbar/2e) (\Omega \text{ m})^{-1}]$ )<sup>[7]</sup>.

**Table S3. The calculated  $\sigma_{SH}$  of samples**

Structure	$\sigma_{SH}(45^\circ)$ [ $\times 10^6 (\hbar/2e) (\Omega \text{ m})^{-1}$ ]	$\sigma_{SH}(-135^\circ)$ [ $\times 10^6 (\hbar/2e) (\Omega \text{ m})^{-1}$ ]
Au/Ni	0.15	0.15
Au/ML WTe <sub>2</sub> /Ni	1.10	1.91
Au/ML MoS <sub>2</sub> /Ni	1.50	2.62

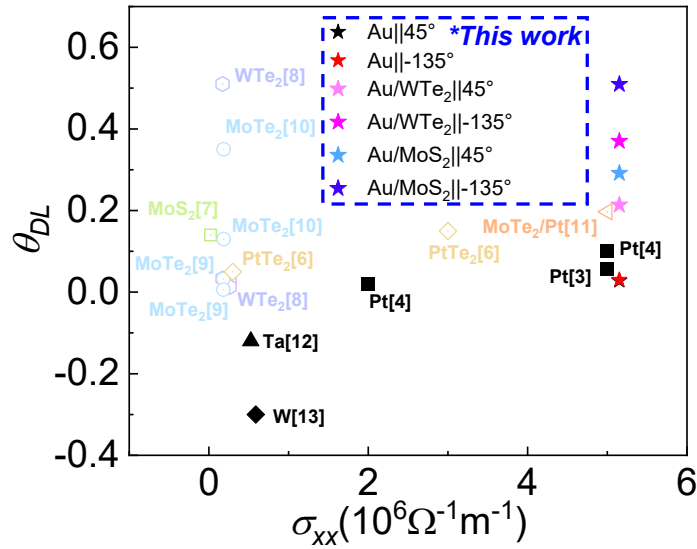


**Figure S5. A comparison of SOT between Au/TMDs (TMDs=MoS<sub>2</sub>, WTe<sub>2</sub>) and other materials.**<sup>[4-5, 7-14]</sup>

#### Reference and notes

- [1] K. Fuchs, *Mathematical Proceedings of the Cambridge Philosophical Society* 1938, **34**, 100-108.
- [2] T. Nan, S. Emori, C. Boone, X. Wang, T. Oxholm, J. Jones, B. Howe, G. Brown, N. Sun, *Phys. Rev. B* 2015, **91**, 214416.
- [3] D. MacNeill, G. M. Stiehl, M. H. D. Guimaraes, R. A. Buhrman, J. Park, D. C. Ralph, *Nat. Phys.* 2016, **13**, 300-305.
- [4] L. Liu, T. Moriyama, D. Ralph, R. Buhrman, *Phys. Rev. Lett.* 2011, **106**, 036601.
- [5] A. Ganguly, K. Kondou, H. Sukegawa, S. Mitani, S. Kasai, Y. Niimi, Y. Otani, A. Barman, *Appl. Phys. Lett.* 2014, **104**, 072405.
- [6] A. Ganguly, R. M. Rowan-Robinson, A. Haldar, S. Jaiswal, J. Sinha, A. T. Hindmarch, D. A. Atkinson, A. Barman, *Appl. Phys. Lett.* 2014, **105**, 112409.
- [7] H. Xu, J. Wei, H. Zhou, J. Feng, T. Xu, H. Du, C. He, Y. Huang, J. Zhang, Y. Liu, H. C. Wu, C. Guo, X. Wang, Y. Guang, H. Wei, Y. Peng, W. Jiang, G. Yu, X. Han, *Adv. Mater.* 2020, **32**, 2000513.
- [8] Q. Shao, G. Yu, Y. W. Lan, Y. Shi, M. Y. Li, C. Zheng, X. Zhu, L. J. Li, P. K. Amiri, K. L. Wang, *Nano Lett.* 2016, **16**, 7514-7520.

- [9] D. MacNeill, G. M. Stiehl, M. H. D. Guimarães, N. D. Reynolds, R. A. Buhrman, D. C. Ralph, *Phys. Rev. B* 2017, **96**, 054450.
- [10] G. M. Stiehl, R. Li, V. Gupta, I. E. Baggari, S. Jiang, H. Xie, L. F. Kourkoutis, K. F. Mak, J. Shan, R. A. Buhrman, D. C. Ralph, *Phys. Rev. B* 2019, **100**, 184402.
- [11] S. Liang, S. Shi, C. H. Hsu, K. Cai, Y. Wang, P. He, Y. Wu, V. M. Pereira, H. Yang, *Adv. Mater.* 2020, **32**, 2002799.
- [12] Q. Chen, W. Lv, S. Li, W. Lv, J. Cai, Y. Zhu, J. Wang, R. Li, B. Zhang, Z. Zeng, *Chin. Phys. B* 2021, **30**, 097506.
- [13] L. Liu, C. Pai, Y. Li, H. Tseng, D. Ralph, R. Buhrman, *Science* 2012, **336**, 555-558.
- [14] J. de la Venta, S. Wang, J. G. Ramirez, I. K. Schuller, *Appl. Phys. Lett.* 2013, **102**, 122404.